J. Phys. A: Math. Gen. **29** (1996) 5359–5373. Printed in the UK

Evolution of a multimodal map induced by an equivariant vector field

C Letellier, P Dutertre, J Reizner and G Gouesbet

LESP, URA CNRS 230, INSA de Rouen, BP 08, Place Emile Blondel, 76131 Mont Saint-Aignan Cedex, France

Received 19 April 1996

Abstract. It has been shown that the topological characterization of an equivariant system should preferably be achieved by working in a fundamental domain generated by the symmetry properties appearing in the phase space. In this paper, we discuss the case when the equivariance of the studied system is taken into account to study the evolution of the population of periodic orbits when a control parameter is varied. The Burke–Shaw system is considered here as an example. It is shown that the equivariance of this system may be used to reduce the multimodal first-return map in a Poincaré section to a unimodal map. A relationship between four-symbol sequences and two-symbol sequences is given. The non-trivial evolution of the orbit spectrum of a multimodal map is then predicted from the much simpler unimodal map to which the multimodal map reduces.

1. Introduction

It is now well known that the set of unstable periodic orbits in a chaotic attractor may be viewed as its skeleton [1]. In recent years, many papers have been devoted to the knowledge of the population of periodic orbits embedded within attractors. In particular, it arises that the population of periodic orbits may be encoded by using symbolic dynamics induced by the generating partition defined by the critical points of a unidimensional first-return map. Then, the population of periodic orbits may be extracted and encoded for fixed values of the control parameters.

In the present paper, the Burke–Shaw system [2] is investigated on a control parameter line. By working in the complete phase space, i.e. without taking into account the equivariance of the system, the Poincaré map is found to be constituted by up to four branches. The description of the evolution of the orbit spectrum when a control parameter is varied is then rather complicated. Conversely, when the equivariance of the vector field is taken into account in the characterization of the attractor, i.e. when the analysis is achieved in a fundamental domain of the phase space [3–5], the evolution of the orbit spectrum is found to be governed by the unimodal order and, consequently, can be completely predicted. A relationship between the symbolic dynamics defined on the whole space and the symbolic dynamics defined in a fundamental domain is given, allowing the prediction of the evolution of the 4-symbol dynamics from the unimodal order.

The paper is organized as follows. Section 2 briefly describes the topological properties of the Burke–Shaw system in the whole phase space and the evolution of the orbit spectrum. In section 3, a study of the evolution of the orbit spectrum is achieved by taking into account the equivariance property of the vector field. It is explained how the description

0305-4470/96/175359+15$19.50

of the evolution of the Burke–Shaw system may be achieved by using the unimodal order. Section 4 is a conclusion.

2. Analysis in the whole phase space

2.1. The Burke–Shaw system

The Burke–Shaw system has been derived by Burke and Shaw from the Lorenz equations [2]. They proposed a set of equations reading as

$$\begin{cases} \dot{x} = -S(x+y) \\ \dot{y} = -y - Sxz \\ \dot{z} = Sxy + V \end{cases} \tag{1}$$

where S and V are the control parameters. The Burke–Shaw system (1) is equivariant under the Z_2 symmetry $\gamma : (x, y, z) \to (-x, -y, z)$:

$$\boldsymbol{f}(\lambda, \gamma\boldsymbol{x}(t)) = \gamma\boldsymbol{f}(\lambda, \boldsymbol{x}(t)) \tag{2}$$

in which $\boldsymbol{x}(t)$ is a real-valued vector, t is the time, λ is the parameter vector and γ is a matrix defining the equivariance. The Burke–Shaw system (1) with parameter vector $\lambda = (S, V)$ and variables $\boldsymbol{x} = (x, y, z)$ is equivariant with the equivariant matrix reading as

$$\gamma = \begin{pmatrix} -1 & 0 & 0 \\ 0 & -1 & 0 \\ 0 & 0 & 1 \end{pmatrix} \tag{3}$$

defining an axial symmetry of $\pm\pi$.

This equivariance is a Z_2-symmetry, i.e. $\gamma^2 = \mathbb{I}$. In other words, the Burke–Shaw system remains globally unchanged if we apply the γ-matrix as follows:

$$(x, y, z) \xrightarrow{\gamma} (-x, -y, z). \tag{4}$$

In this paper, S is taken to be equal to 10 and V is the variable control parameter ranging on [3.0, 4.272]. The system possesses two fixed points $F_\pm$ given by

$$\begin{cases} x_\pm = \pm\sqrt{\dfrac{V}{S}} \\ y_\pm = \mp\sqrt{\dfrac{V}{S}} \\ z_\pm = \dfrac{1}{S}. \end{cases} \tag{5}$$

For $V = 4.272$, the asymptotic motion settles down onto a strange chaotic attractor displayed in figure 1: this statement is based on computer experiment.

2.2. Topological characterization

The topological approach is based on the organization of periodic orbits whose linking properties severely constrain the topology of strange attractors. In particular, in three-dimensional spaces, periodic orbits may be viewed as knots [6]. A quantitative topological characterization of low-dimensional chaotic sets requires the assignment of a good symbolic encoding of trajectories which is given by a first-return map built on the Poincaré section P defined as follows

$$P \equiv \{(x, y) \in \mathbb{R}^2 | z = z_\pm,\ x > 0,\ \dot{z} < 0\}. \tag{6}$$

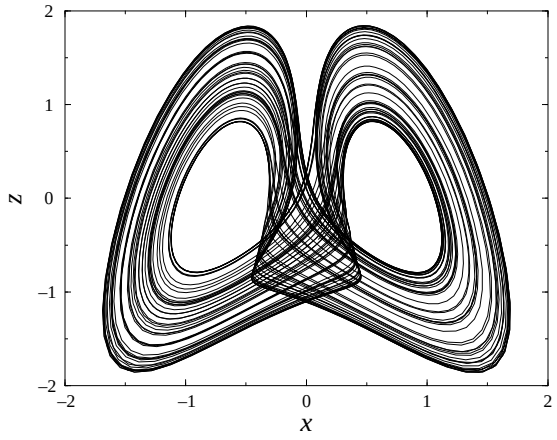

Figure 1. Chaotic attractor generated by the Burke–Shaw system for $(S, V) = (10, 4.272)$.

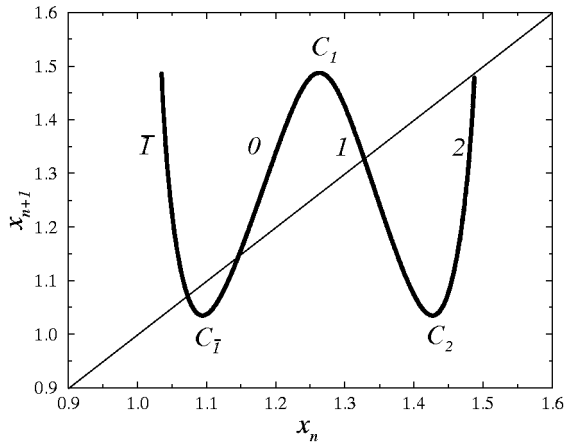

Figure 2. First-return map to the Poincaré section P for $V = 4.272$. The absence of any layered structure in this one-dimensional map is a signature of the high dissipative properties of the dynamical system and is a justification of the use of the reduced map.

The Poincaré plane then contains the fixed point F_+. The vector field defined by equations (1) is strongly dissipative and, consequently, the two-dimensional map is reduced to a one-dimensional map. From this Poincaré section P, a first-return map is then computed and displayed in figure 2. Four branches are exhibited. Let us label them on the set $\S_4 = \{\bar{1}, 0, 1, 2\}$. This labelling is chosen to exhibit the symmetry properties inherent to the Burke–Shaw system in terms of symbolic sequences (see section 2.4). Periodic orbits will be encoded according to this generating partition.

A mask of the attractor, which may be viewed as the knot-holder of the Burke–Shaw attractor (i.e. as a manifold with a boundary in which knots are embedded), is built after many visual investigations in the tridimensional state space, as displayed in figure 3. This mask is related to a stretched and folded band on which asymptotic trajectories evolve in the state space. Such an approach may be used whenever the vector field is strongly dissipative

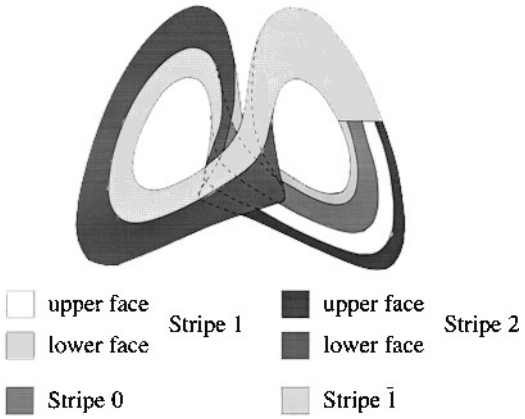

Figure 3. Mask of the Burke–Shaw attractor for $V = 4.272$.

and tridimensional and was first introduced by Birman and Williams on the Lorenz system [7]. From the mask, we are able to define four strips, each one being associated with a branch of the first-return map. An increasing branch is associated with a strip undergoing an even number of π-twists while a decreasing branch corresponds to a strip undergoing an odd number of π-twists.

Once the mask is extracted (figure 3), the topology is synthetized in a template as explained in [8]. A template may be described by a linking matrix M_{ij} in which M_{ij} is the local torsion (the number of oriented π-twists) of the ith strip if $i = j$, and the sum of the oriented crossings between the ith and the jth strips if $i \neq j$. In our case, the template presents four strips (figure 4) and, consequently, the linking matrix is a 4×4 matrix. The local torsions in the template are in agreement with the branches of the first-return map, i.e. strips $\bar{1}$ and 1 which are associated with the decreasing branches possess an odd local torsion and strips 0 and 2 which are associated with the increasing branches possess an even local torsion. The linking matrix of the Burke–Shaw template reads as

$$M_{ij} = \begin{pmatrix} +3 & +2 & +2 & +3 \\ +2 & +2 & +2 & +3 \\ +2 & +2 & +3 & +3 \\ +3 & +3 & +3 & +4 \end{pmatrix}. \tag{7}$$

This template has been checked by evaluating a few linking numbers on plane projections of orbit couples. All linking numbers evaluated from plane projections have been found to be equal to the ones predicted by the template. Details concerning such a topological characterization procedure may be found in [6] or in [8]. This topological characterization is based on linking numbers which are invariant under isotopy of knots, i.e. a continuous deformation of knots without any cutting. Linking numbers between two periodic orbits are therefore preserved under a control parameter change as long as the orbits remain embedded within the attractor.

2.3. Multimodal maps and order relations

In the last few decades, several works have been devoted to the study of a unimodal map under the variation of a control parameter. From pioneering papers by Metropolis *et al* [9], Collet and Eckmann [10] or Hao Bai Lin [11] to the recent paper by Hall [12], a symbolic

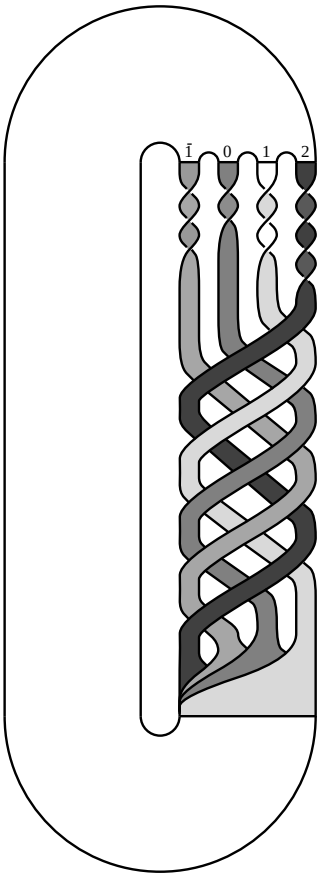

Figure 4. Template of the Burke–Shaw attractor for $V = 4.272$.

dynamics and a unimodal order are introduced to describe the creation of periodic orbits.

Let us recall some basic statements. In the case of a strongly dissipative unimodal map F_μ, one critical point C separates an increasing branch and a decreasing branch, labelled 0 and 1, respectively. Then each point x_n of the invariant set of the map possesses a code $K(x_n) = \sigma_n$ defined by

$$\sigma_n = \begin{cases} 0 & \text{if } x_n < C \\ 1 & \text{if } x_n > C. \end{cases} \tag{8}$$

Consequently, a trajectory starting from x_1 with $K(x_1) = \sigma_1$ may be encoded by a symbolic sequence constituted by the string of the successive codes on $\S_2 = \{0, 1\}$ reading as

$$S = \sigma_1\sigma_2 \ldots \sigma_i \ldots$$

In a period-p orbit, a sub-string $\bar{S}$ of S is infinitely repeated. Clearly, the sub-string $\bar{S}$ contains p codes and reads as

$$\bar{S} = \sigma_1\sigma_2 \ldots \sigma_p$$

with $\sigma_1 = \sigma_{p+1}$.

A periodic orbit may then be encoded by a symbolic sequence (W) which is given by a sub-string $\bar{S}$. To the ith periodic point of such a periodic orbit encoded by (W) may be associated a symbolic sequence W_i reading as

$$W_i = \sigma_i \sigma_{i+1} \dots \sigma_p \sigma_1 \dots \sigma_{i-1}$$

where W_i is the cyclic permutation of (W) whose σ_i is the code of the ith point.

All periodic points may be ordered by the unimodal order $\prec_1$ [10, 12] which is defined as follows.

Let us consider two symbolic sequences

$$W_1 = \sigma_1 \sigma_2 \dots \sigma_k \sigma_{k+1} \dots$$

and

$$W_2 = \tau_1 \tau_2 \dots \tau_k \tau_{k+1} \dots$$

where σ_i's and τ_j's designate codes on $\S_2$. Suppose $\sigma_i = \tau_i$ for all $i < k$ and $\sigma_k \neq \tau_k$. Let $W^* = \sigma_1 \dots \sigma_{k-1} = \tau_1 \dots \tau_{k-1}$ be the common part between W_1 and W_2. Setting that a string $\sigma_1 \sigma_2 \dots \sigma_{k-1}$ is even (odd) if the sum $\sum_{i=1}^{k-1} \sigma_i$ is even (odd), then we have

$$\begin{cases} W_1 \prec_1 W_2 & \text{if } W^* \text{ is even and } \sigma_k < \tau_k \\ W_1 \prec_1 W_2 & \text{if } W^* \text{ is odd and } \tau_k < \sigma_k \\ W_2 \prec_1 W_1 & \text{if } W^* \text{ is odd and } \sigma_k < \tau_k \\ W_2 \prec_1 W_1 & \text{if } W^* \text{ is even and } \tau_k < \sigma_k. \end{cases}$$

If W_1 and W_2 do not start with any common part, then W^* is assumed to be even. When $W_2 \prec_1 W_1$, we say that W_1 implies W_2.

When a period-p orbit of a map F_μ is created for $\mu = \mu^*$, the p periodic points x_i satisfy

$$x_i = F^i_{\mu^*}(x_C) \qquad \text{for } i \in [1, p] \tag{9}$$

in which x_C is the coordinate of the periodic point appearing at the tangent bifurcation creating the periodic orbit (closest to the critical point C). Clearly, $x_p = x_C$. The symbolic sequence

$$(W) = \sigma_1 \dots \sigma_p$$

where σ_i's are the codes of the p periodic points x_i (the code of the critical point C may be taken equal to either 0 or 1) is here called the *orbital sequence*. When an orbital sequence (W_1) implies an orbital sequence (W_2), we say that (W_1) *forces* (W_2) and we note $(W_2) \prec_2 (W_1)$ where $\prec_2$ is the *forcing order*. Let us note here that the forcing order is therefore defined by using the same rules as for the unimodal order. However, for the sake of clarity, it is convenient to introduce two different notations for implying and for forcing.

For a unidimensional unimodal map, the orbital sequence (W) is always the cyclic permutation W_i which implies the $(p-1)$ others. Moreover, at $\mu = \mu^*$, the orbital sequence (W) of the newly born orbit forces all the orbital sequences of periodic orbits which are present within the invariant set. The orbital sequence (W) is also called the *kneading sequence* for $\mu = \mu^*$ and is denoted $(\overline{W})$.

These concepts may be extended to multimodal maps [13, 11]. In the case of the multimodal map induced by the Burke–Shaw system, three critical points are present. Orbits

are therefore encoded on $\S_4$ according to

$$\sigma_n = \begin{cases} \bar{1} & \text{if } x_n < x_{C_{\bar{1}}} \\ 0 & \text{if } x_{C_{\bar{1}}} < x_n < x_{C_1} \\ 1 & \text{if } x_{C_1} < x_n < x_{C_2} \\ 2 & \text{if } x_{C_2} < x_n \end{cases} \tag{10}$$

where C_i $(i = \bar{1}, 1, 2)$ denote the critical points.

We may then possibly define a multimodal implying order and a multimodal forcing order by using the same rule as previously given for the unimodal order but with the codes now taken on $\S_4$. Unfortunately, such orders are not so useful as the unimodal order since, in the general case, the sequence of bifurcations of a multimodal map is different from the one of an ideal family of multimodal maps, i.e. satisfying the aforementioned multimodal orders. Thus, the admissibility conditions for a symbolic sequence W must be defined in a more general way.

A periodic orbit encoded by the sequence W of p symbols taken on $\S_4$ will be admissible if each one of its p cyclic permutations

$$W_i = \sigma_i \sigma_{i+1} \ldots \sigma_p \sigma_1 \ldots \sigma_{i-1}$$

satisfies the conditions depending on the code σ_{i-1}:

$$\begin{cases} K_{\bar{1}} <_1 W_i & \text{if } \sigma_{i-1} = \bar{1} \text{ or } \sigma_{i-1} = 0 \\ W_i <_1 K_1 & \text{if } \sigma_{i-1} = 0 \text{ or } \sigma_{i-1} = 1 \\ K_2 <_1 W_i & \text{if } \sigma_{i-1} = 1 \text{ or } \sigma_{i-1} = 2 \end{cases}$$

where $K_{\bar{1}}$, K_1 and K_2 are the kneading sequences associated with the critical points $C_{\bar{1}}$, C_1 and C_2, respectively. The orbit spectrum of an attractor is then constituted by the set of all admissible periodic orbits. When the control parameters are varied, the kneading sequences associated with each critical point change and, consequently, the orbit spectrum evolves.

2.4. Evolution of the orbit spectrum

For $V = 3.0$, there exist two limit cycles on which the asymptotic motion settles down depending on the initial conditions. These two limit cycles are displayed in figure 5. They are labelled $A_{\bar{1}}$ and A_1, respectively.

When the control parameter V is increased, these two limit cycles lose their stability through period-doubling bifurcations. Two simultaneous cascades of period-doublings then arise which, in terms of symbolic dynamics, are described as follows:

$\bar{1}$	1	$V = 2.831$
$\bar{1}0$	10	$V = 3.448$
$\bar{1}0\bar{1}\bar{1}$	1011	$V = 3.589$
$\bar{1}0\bar{1}\bar{1}$ $\bar{1}0\bar{1}0$	1011 1010	$V = 3.621$
$\bar{1}0\bar{1}\bar{1}$ $\bar{1}0\bar{1}0$ $\bar{1}0\bar{1}\bar{1}$ $\bar{1}0\bar{1}\bar{1}$	1011 1010 1011 1011	$V = 3.628.$

The accumulation point is reached for $V \approx 3.629$. Beyond this value, the asymptotic behaviour settles down onto one of the two chaotic attractors A_1 and $A_{\bar{1}}$ depending on the initial conditions. The first-return map of these attractors is displayed entirely in figure 6.

Periodic orbits of each attractor are encoded according to the partition induced by the critical point of the associated first-return map. Thus, periodic orbits of attractor $A_{\bar{1}}$ are encoded on the set $\S_2^* = \{\bar{1}, 0\}$ and orbits of A_1 on $\S_2 = \{0, 1\}$. Because the route to chaos is

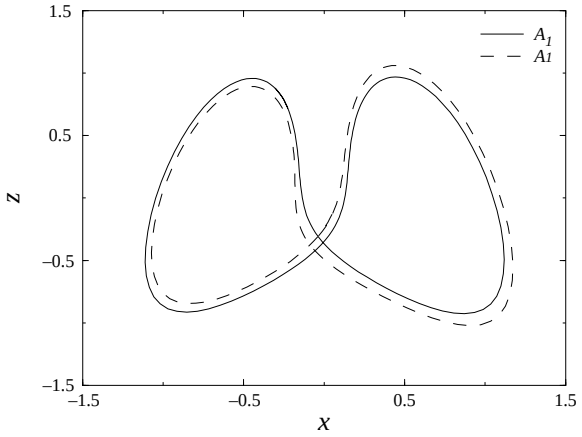

Figure 5. Coexistence of two limit cycles.

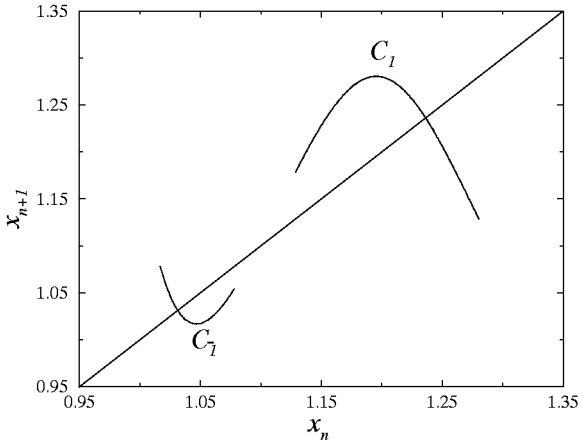

Figure 6. First-return maps of the two co-existing attractors, corresponding to $A_{\bar{1}}$ on the left and to A_1 on the right.

the period-doubling cascade, the creation of periodic orbits under the increase of the control parameter V is governed by the unimodal forcing order [10, 12, 14]. For $V = 3.8115$, however, a boundary crisis arises and the two attractors collide to form a single larger attractor. This scenario has been described by Gregobi *et al* [15]. At this V-value, the first-return map (figure 7) is then constituted by three monotonic branches labelled $\bar{1}$, 0 and 1.

As could be expected from the simultaneity of the period-doubling cascades associated with the two attractors, the first-return map is symmetric, in terms of allowed symbolic sequences, with respect to the period-1 orbit encoded by (0). Indeed, the attractor A_1 is symmetrical to $A_{\bar{1}}$ under the action of the γ-matrix. The map is symmetric up to the boundary crisis which appears for $V = 3.8115$. Both attractors then become a single symmetric attractor. Beyond this V-value, the symmetry is broken and the evolution of the orbit spectrum cannot be compared to the evolution of a symmetric map.

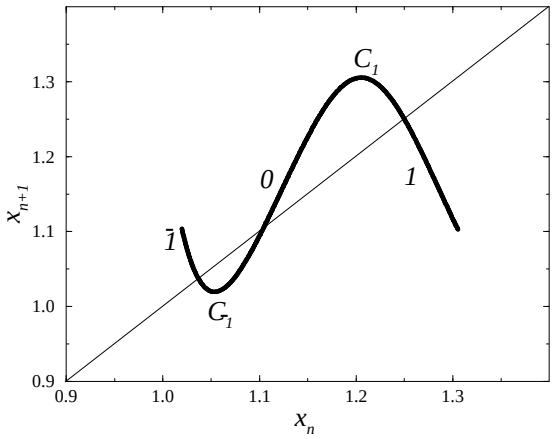

Figure 7. The three-branched map for $V = 3.8115$.

With many numerical computations, the order of creation of periodic orbits is studied and reported in table 1 for $V \in [3, 4.272]$. We then observe that, just beyond the boundary crisis, the first two orbits to be created may be written as

$$C_{\bar{1}}(\bar{1}0^0_1 1^0_{\bar{1}})_{C_1}.$$

They are easily found in the table since they are the first orbits to be encoded with three different symbols. A pitchfork bifurcation is hereafter observed. It destabilizes the orbit encoded by $C_{\bar{1}}(\bar{1}011\bar{1})_{C_1}$. Two limit cycles then coexist, encoded by $(\bar{1}0110)_{C_{\bar{1}}}$ and $(1\bar{1}\bar{1}00)_{C_1}$. These two limit cycles then generate two simultaneous period-doubling cascades.

3. Analysis in the fundamental domain

3.1. Topological characterization

Above, we have developed a topological analysis of the Burke–Shaw system in the whole state space as is common practice. From such an analysis in the whole state space, the Burke–Shaw system could be described in terms of a multimodal map. The evolution of the orbit spectrum could then be studied by using a symbolic dynamics requiring four symbols. Moreover, as the first-return map is symmetric in terms of symbolic sequences, such a study would be achieved in a similar way as the one introduced by Fang [16] for the study of antisymmetrical maps. When this program is fulfilled, it is observed that the order of creation of periodic orbits is rather intricate, and cannot be easily predicted. Conversely, in this subsection, we show that a very easy prediction can be achieved if we take into account the equivariance properties of the Burke–Shaw system.

In previous papers [4, 5], we have shown that, in the presence of equivariant properties, a system is preferably analysed in a fundamental domain defined with respect to the symmetry properties of the phase portrait, i.e. such a fundamental domain may be used to tesselate the whole attractor. The specific procedure required to characterize equivariant systems is completely reported in [4] with the Lorenz system taken as an example (see also [5] for the more general case of covers of the proto-Lorenz system). In this case, a wing of the Lorenz attractor may roughly be viewed as the fundamental domain $\mathcal{D}$. The whole attractor is then

Table 1. Order of creation of orbits with period smaller than 6, extracted from the Burke–Shaw system for $V \in [3, 4.272]$.

$(W)_{c_2}$	$(W)_{c_{\bar{1}}}$	$c_j(W)c_i$	$(W)_{c_1}$	$(W)_{c_2}$	$(W)_{c_{\bar{1}}}$	$c_j(W)c_i$	$(W)_{c_1}$
	$\overset{0}{\bar{1}}$		$\overset{0}{1}$		$\bar{1}2\bar{1}1\overset{\bar{1}}{0}$		$2120\overset{1}{0}$
	$\bar{1}0$		10	$\bar{1}2\bar{1}1\overset{1}{2}$			$212\bar{1}\overset{0}{1}$
	$\bar{1}0\bar{1}\bar{1}$		1011	$\bar{1}2\bar{1}0\overset{2}{1}$			$211\bar{1}\overset{1}{0}$
	$\bar{1}0\bar{1}\bar{1}\overset{\bar{1}}{0}$		$1011\overset{1}{0}$		$\bar{1}2\bar{1}0\overset{0}{\bar{1}}$		$2110\overset{0}{1}$
	$\bar{1}0\overset{\bar{1}}{0}$		$10\overset{1}{0}$		$\bar{1}21\overset{0}{\bar{1}}$		$211\overset{0}{1}$
	$\bar{1}00\overset{0}{\bar{1}}$		$1001\overset{0}{1}$		$\bar{1}2\bar{1}\bar{1}\overset{\bar{1}}{0}$		$2111\overset{1}{0}$
	$\bar{1}00\overset{\bar{1}}{0}$		$100\overset{1}{0}$	$\bar{1}2\bar{1}\bar{1}\overset{1}{2}$			$2112\overset{0}{1}$
	$\bar{1}000\overset{\bar{1}}{0}$		$1000\overset{1}{0}$		$\bar{1}2\overset{\bar{1}}{0}$		$21\overset{1}{0}$
		$c_{\bar{1}}(\bar{1}0\overset{0}{1}1\overset{0}{\bar{1}})c_1$		$\bar{1}20\bar{1}\overset{2}{1}$			$2102\overset{1}{0}$
	$\bar{1}0110$		$1\bar{1}\bar{1}00$		$\bar{1}20\bar{1}\overset{0}{\bar{1}}$		$2101\overset{0}{1}$
	$\bar{1}010\overset{0}{\bar{1}}$		$1\bar{1}00\overset{0}{1}$		$\bar{1}20\overset{\bar{1}}{0}$		$210\overset{1}{0}$
	$\bar{1}01\overset{0}{\bar{1}}$		$1\bar{1}0\overset{0}{1}$		$\bar{1}200\overset{\bar{1}}{0}$		$2100\overset{1}{0}$
	$\bar{1}01\bar{1}\overset{\bar{1}}{0}$		$1\bar{1}01\overset{1}{0}$	$\bar{1}200\overset{1}{2}$			$210\bar{1}\overset{0}{1}$
		$c_1(\bar{1}\overset{0}{1}\overset{1}{2})c_2$		$\bar{1}201\overset{2}{1}$			$21\bar{1}\bar{1}\overset{1}{0}$
$\bar{1}11$			$2\bar{1}0$		$\bar{1}201\overset{0}{\bar{1}}$		$21\bar{1}0\overset{0}{1}$
	$\bar{1}11\bar{1}\overset{0}{\bar{1}}$		$2\bar{1}01\overset{0}{1}$	$\bar{1}20\overset{1}{2}$			$21\bar{1}\overset{0}{1}$
	$\bar{1}11\overset{\bar{1}}{0}$		$2\bar{1}0\overset{1}{0}$		$\bar{1}202\overset{\bar{1}}{0}$		$21\bar{1}1\overset{1}{0}$
	$\bar{1}110\overset{\bar{1}}{0}$		$2\bar{1}00\overset{1}{0}$			$c_1(\bar{1}2\overset{0}{1}2\overset{1}{2})c_2$	
$\bar{1}110\overset{1}{2}$			$2\bar{1}0\bar{1}\overset{0}{1}$	$\bar{1}2121$			$22\bar{1}20$
$\bar{1}111\overset{2}{1}$			$2\bar{1}\bar{1}\bar{1}\overset{1}{0}$		$\bar{1}212\overset{0}{\bar{1}}$		$22\bar{1}1\overset{0}{1}$
	$\bar{1}111\overset{0}{\bar{1}}$		$2\bar{1}\bar{1}0\overset{0}{1}$	$\bar{1}21\overset{2}{1}$			$22\bar{1}\overset{1}{0}$
$\bar{1}11\overset{1}{2}$			$2\bar{1}\bar{1}\overset{0}{1}$		$\bar{1}211\overset{\bar{1}}{0}$		$22\bar{1}0\overset{0}{1}$
		$c_{\bar{1}}(\bar{1}1\overset{1}{0}2\overset{\bar{1}}{0})c_1$		$\bar{1}211\overset{1}{2}$			$22\bar{1}\bar{1}\overset{0}{1}$
	$\bar{1}1021$		$20\bar{1}11$	$\bar{1}210\overset{2}{1}$			$220\bar{1}\overset{1}{0}$
$\bar{1}10\overset{2}{1}$			$20\bar{1}\overset{1}{0}$		$\bar{1}210\overset{0}{\bar{1}}$		$2200\overset{0}{1}$
	$\bar{1}101\overset{\bar{1}}{0}$		$20\bar{1}0\overset{1}{0}$		$\bar{1}21\overset{0}{\bar{1}}$		$220\overset{0}{1}$
$\bar{1}101\overset{1}{2}$			$20\bar{1}\bar{1}\overset{0}{1}$		$\bar{1}21\bar{1}\overset{\bar{1}}{0}$		$2201\overset{1}{0}$
$\bar{1}100\overset{2}{1}$			$200\bar{1}\overset{1}{0}$	$\bar{1}21\bar{1}\overset{1}{2}$			$2202\overset{0}{1}$
	$\bar{1}100\overset{0}{\bar{1}}$		$2000\overset{0}{1}$	$\bar{1}2\overset{1}{2}$			$22\overset{0}{1}$
	$\bar{1}10\overset{0}{\bar{1}}$		$200\overset{0}{1}$	$\bar{1}22\bar{1}\overset{2}{1}$			$2212\overset{1}{0}$
	$\bar{1}10\bar{1}\overset{\bar{1}}{0}$		$2001\overset{1}{0}$		$\bar{1}22\bar{1}\overset{0}{\bar{1}}$		$2211\overset{0}{1}$
	$\bar{1}1\overset{0}{\bar{1}}$		$20\overset{0}{1}$		$\bar{1}22\overset{\bar{1}}{0}$		$221\overset{1}{0}$
	$\bar{1}1\bar{1}\bar{1}\overset{0}{\bar{1}}$		$2011\overset{0}{1}$		$\bar{1}220\overset{\bar{1}}{0}$		$2210\overset{1}{0}$
	$\bar{1}1\bar{1}\overset{\bar{1}}{0}$		$201\overset{1}{0}$	$\bar{1}220\overset{1}{2}$			$221\bar{1}\overset{0}{1}$
	$\bar{1}1\bar{1}0\overset{\bar{1}}{0}$		$2010\overset{1}{0}$	$\bar{1}221\overset{2}{1}$			$222\bar{1}\overset{1}{0}$
$\bar{1}1\bar{1}0\overset{1}{2}$			$201\bar{1}\overset{0}{1}$		$\bar{1}221\overset{0}{\bar{1}}$		$2220\overset{0}{1}$
$\bar{1}1\bar{1}1\overset{2}{1}$			$202\bar{1}\overset{1}{0}$	$\bar{1}22\overset{1}{2}$			$222\overset{0}{1}$
	$\bar{1}1\bar{1}1\overset{0}{\bar{1}}$		$2020\overset{0}{1}$		$\bar{1}222\overset{\bar{1}}{0}$		$2221\overset{1}{0}$
$\bar{1}\overset{1}{2}$			$2\overset{0}{1}$	$\bar{1}222\overset{1}{2}$			$2222\overset{0}{1}$
$\bar{1}2\bar{1}1$			2120				

tiled by the fundamental domain $\mathcal{D}$ (say the right wing) and one of its copy (say the left wing).

In the presence of equivariance properties, it has then been demonstrated that the relevant topology is the topology of the fundamental domain rather than the topology of the whole attractor [5]. Consequently, the dynamics is characterized by a fundamental template whose extraction is now given.

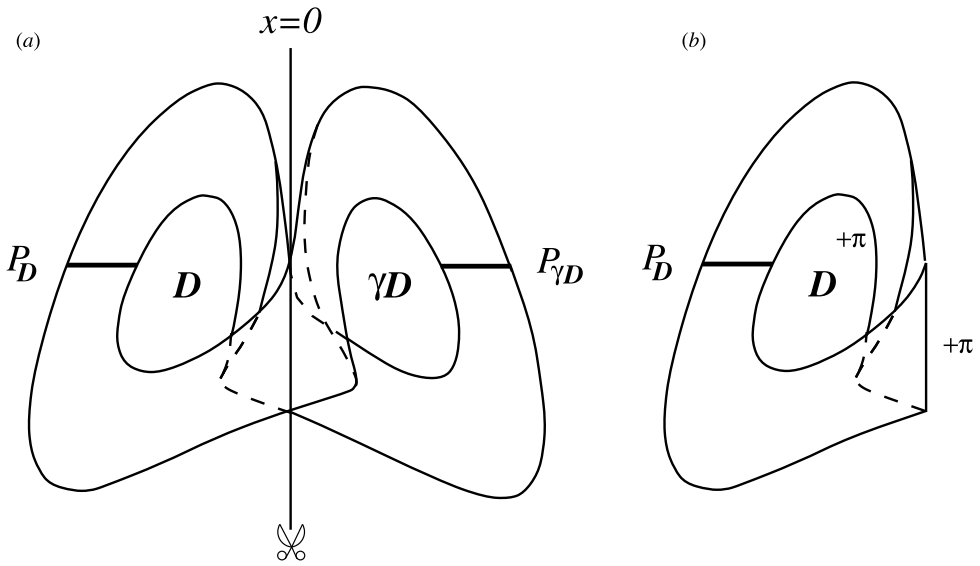

Figure 8. The mask of the fundamental domain $\mathcal{D}$ is built by isolating $\mathcal{D}$ from the original mask and gluing the outcoming strip with the incoming strip. (*a*) Mask of the Burke–Shaw attractor; (*b*) mask of the fundamental domain $\mathcal{D}$.

Starting from the original mask displayed in figure 8(*a*), a mask of the fundamental domain is built (figure 8(*b*)). The fundamental domain is easily isolated since the axis of symmetry is the z-axis. Thus, on an xz-plane projection of the attractor (or on the mask displayed in figure 8(*a*)), the fundamental domain $\mathcal{D}$ is separated from its copy $\gamma\mathcal{D}$ by the line $x = 0$. From the fundamental mask displayed in figure 8(*b*), two strips are exhibited. The first strip, labelled 0, undergoes two successive positive π-twists while the second strip, labelled 1, presents a single positive π-twist. The fundamental template is then found to be defined by the linking matrix

$$M_{\mathcal{D}} = \begin{pmatrix} +2 & +1 \\ +1 & +1 \end{pmatrix}. \tag{11}$$

The fundamental template is displayed in figure 9. The existence and properties of the two strips are confirmed by a first-return map to a Poincaré set P defined as the union of the Poincaré sections

$$P_{\mathcal{D}} = \{(x, y) \in \mathbb{R}^2 | z = z_{\pm},\ \dot{z} < 0,\ x > x_+\} \tag{12}$$

and

$$P_{\gamma\mathcal{D}} = \{(x, y) \in \mathbb{R}^2 | z = z_{\pm},\ \dot{z} > 0,\ x < x_-\} \tag{13}$$

in which the identification between $\mathcal{D}$ and $\gamma\mathcal{D}$ (figure 8(*a*)) defines an invariant variable $|x|$. Indeed, the first-return map computed with the invariant variable $|x|$ exhibits two monotonic branches (figure 10). The increasing branch is associated with strip 0 which

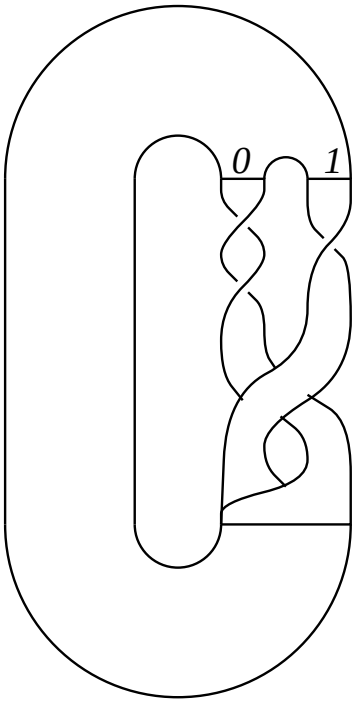

Figure 9. Fundamental template of the Burke–Shaw attractor for $V = 4.272$.

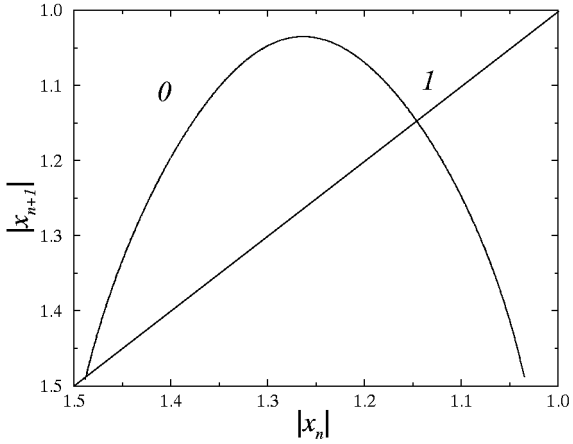

Figure 10. First-return map to the Poincaré set P built with the invariant variable $|x|$.

presents an even number of π-twists, while the decreasing branch corresponds to strip 1 which undergoes one π-twist. Consequently, periodic orbits are now encoded on the set $\S_2^{\mathcal{D}} = \{0, 1\}$. Moreover, the first-return map presents a logistic map structure which causes the period-doubling cascade to be the route to chaos. Such a result is of crucial relevance since the evolution of the population of periodic orbits must therefore be exactly predicted by the unimodal order.

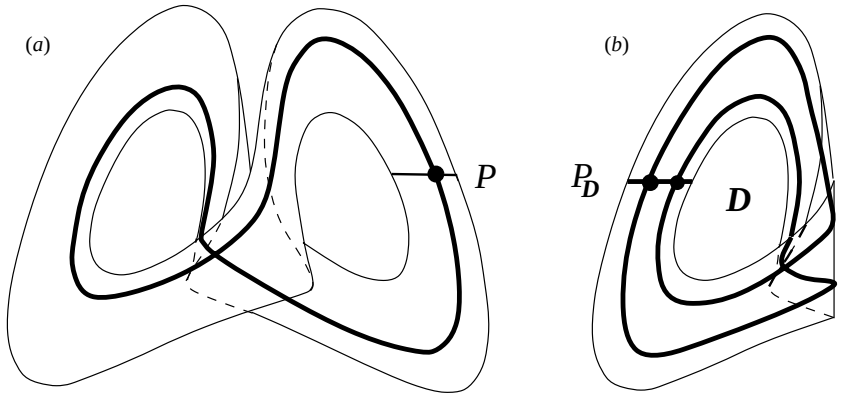

Figure 11. Evolution of the period of an orbit under the action of Φ which projects the dynamics on the fundamental domain. (a) Orbit encoded by (1) on the whole attractor; (b) the same orbit projected on the fundamental domain $\mathcal{D}$. It is now encoded by (10).

3.2. Description of the evolution of orbit spectrum

We have now to establish a relationship between the symbolic dynamics defined on the whole attractor and the symbolic dynamics defined on the fundamental domain $\mathcal{D}$. To this purpose, we first remark that the projection of the dynamics on the fundamental domain induces a multiplication by two of the period of each orbit [5]. For instance, let us consider the orbit encoded by (1) on the whole attractor (figure 11(a)). When this orbit is projected on the fundamental domain $\mathcal{D}$, it presents two intersections with the Poincaré set P and is therefore of period-2 (figure 11(b)). It is then concluded that a symbol from the set $\S_2^{\mathcal{D}}$ is mapped to a block of two symbols of the set $\S_4$. After many investigations, we found that such a map Φ can be taken as

$$\begin{cases} \Phi(\bar{1}) = 10 \\ \Phi(0) = 11 \\ \Phi(1) = 01 \\ \Phi(2) = 00 \end{cases} \tag{14}$$

where one may see that Φ maps symbols in blocks of the same parity. For instance, the orbit encoded by ($\bar{1}11$) on the set $\S_4$ will be encoded by $\tilde{\Phi}(\bar{1}11) = (100101)$ on the set $\S_2^{\mathcal{D}}$.

Let us now remark that the equivariance of the Burke–Shaw system implies that there exist two kinds of periodic orbits: (i) symmetric orbits which are globally invariant under the action of the γ-matrix and (ii) asymmetric orbits which appear by pairs with one orbit of the pair mapped to the other under the action of the γ-matrix. In contrast with asymmetric orbits, symmetric orbits may be written as

$$(W^*\overline{\sigma}_p\overline{W}^*\sigma_p)$$

where W^* is a substring of symbols taken on the set $\S_2$ and $\overline{W}^*$ is the conjugate of W^*, i.e. corresponding to the interchange between 1 and $\bar{1}$. For asymmetric orbits, it is found that the symbolic sequences in $\S_4$ of a pair of orbits are mapped to the same sequence in $\S_2^{\mathcal{D}}$. For instance, from table 1, we find that the orbit ($\bar{1}11$) is paired with the orbit ($2\bar{1}0$) which are both mapped to (100101). Therefore, as expected, projecting the dynamics on the fundamental domain $\mathcal{D}$ mods out the symmetry properties.

Table 2. Prediction of the evolution of the orbit spectrum of the Burke–Shaw system on the range [3.0, 4.272] from the unimodal order. The order of creation may be favourably compared with the one given in table 1 where orbits are paired when required. Certain orbits are not present in this table since they are obtained from higher periodic orbits. Let us note the exception that orbit 1 is not mapped to an orbit whose period is doubled due to the fact that 1 identifies with (11) which is mapped to 0 by relation (15).

$(W)_{S_2^{\mathcal{D}}}$	$\tilde{\Phi}^{-1}(W)$		$(W)_{S_2^{\mathcal{D}}}$	$\tilde{\Phi}^{-1}(W)$			
1		0		10011		$\bar{1}1020$	
10	$\bar{1}$		1	100111	$\bar{1}10$		200
1011	$\bar{1}0$		10	100110	$\bar{1}1\bar{1}$		201
101110	$\bar{1}0\bar{1}$		101	1001	$\bar{1}1$		20
101111	$\bar{1}00$		100	1000	$\bar{1}2$		21
10111		$\bar{1}0010$		100010	$\bar{1}2\bar{1}$		211
10110		$\bar{1}011\bar{1}$		100011	$\bar{1}20$		210
101		$\bar{1}01$		10001		$\bar{1}2021$	
100		112		10000		$\bar{1}2122$	
100101	$\bar{1}11$		$2\bar{1}0$	100001	$\bar{1}21$		220
10010		$\bar{1}112\bar{1}$		100000	$\bar{1}22$		221

The inverse map Φ^{-1} is defined as

$$\begin{cases} \Phi^{-1}(10) = \bar{1} \\ \Phi^{-1}(11) = 0 \\ \Phi^{-1}(01) = 1 \\ \Phi^{-1}(00) = 2 \end{cases} \tag{15}$$

which leads to a unique result, modulo a Bernoulli shift.

For instance, if Φ^{-1} is applied to the sequence (100101) on $\S_2^{\mathcal{D}}$, we obtain $\Phi^{-1}(100101) = (\bar{1}11)$. But we also have to predict the paired orbit. This is achieved by applying a one-step Bernoulli shift to the original sequence on $\S_2^{\mathcal{D}}$. Such a Bernoulli mapping corresponds to a switching from the Poincaré section $P_{\mathcal{D}}$ to the Poincaré section $P_{\gamma\mathcal{D}}$. We then obtain $\Phi^{-1}(001011) = (2\bar{1}0)$ which is indeed the orbit symmetrical to $(\bar{1}11)$.

The evolution of the orbit spectrum of the Burke–Shaw system can now easily be predicted from the unimodal order (see table 2). We have here a demonstration of the importance of symmetry properties in a system and, in particular, of the simplification of the understanding of a system when the equivariance is taken into account in the topological analysis.

4. Conclusion

By using the symmetry properties inherent to the Burke–Shaw system, we demonstrated that its four-branch map may be reduced to a unimodal map whose structure is similar to the well known logistic map. Consequently, the rather complicated evolution of the population of periodic orbits encoded with four symbols is directly predicted from the unimodal order. We then proved that moding out the symmetry by working in a fundamental domain defined with respect to the equivariance order allows us to simplify the analysis of equivariant dynamical systems.

References

[1] Cvitanović P 1991 Periodic orbits as the skeleton of classical and quantum chaos *Physica* **51D** 138–51
[2] Shaw R 1981 Strange attractor, chaotic behaviour and information flow *Z. Naturf.* a **36** 80–112
[3] Cvitanović P and Eckhardt B 1993 Symmetry decomposition of chaotic dynamics *Nonlinearity* **6** 277–311
[4] Letellier C, Dutertre P and Gouesbet G 1994 Characterization of the Lorenz system taking into account the equivariance of the vector field *Phys. Rev.* E **49** 3492–5
[5] Letellier C and Gouesbet G 1995 Topological characterization of a system with high-order symmetries: the proto-Lorenz system *Phys. Rev.* E **52** 4754–61
[6] Tufillaro N B, Abbott T and Reilly J 1992 *An Experimental Approach to Nonlinear Dynamics and Chaos* (New York: Addison-Wesley)
[7] Birman J S and Williams R F 1983 Knotted periodic orbits in dynamical systems: Lorenz's equations *Topology* **22** 47–82
[8] Mindlin G B, Solari H G, Natiello M A, Gilmore R and Hou X J 1991 Topological analysis of chaotic time series data from the Belousov–Zhabotinski reaction *J. Nonlinear Sci.* **1** 147–73
[9] Metropolis N, Stein M L and Stein P R 1973 On finite limit sets for transformations on the unit interval *J. Comb. Theor.* A **15** 25–44
[10] Collet P and Eckmann J P 1980 Iterated maps on the interval as dynamical systems *Progress in Theoretical Physics* ed A Jaffe and D Ruelle (Boston, MA: Birkhäuser)
[11] Lin H B 1989 *Elementary Symbolic Dynamics and Chaos in Dissipative Systems* (Singapore: World Scientific)
[12] Hall T 1994 The creation of horseshoes *Nonlinearity* **7** 861–924
[13] Xie F-G 1994 Symbolic dynamics for the general quartic map *Commun. Theor. Phys.* **22** 43–52
[14] Letellier C, Dutertre P and Maheu B 1995 Unstable periodic orbits and templates of the Rössler system: toward a systematic topological characterization *Chaos* **5** 272–81
[15] Gregobi C, Ott E and Yorke J A 1983 Crises, sudden changes in chaotic attractors, and transient chaos *Physica* **7D** 181–200
[16] Fang H P 1994 Dynamics for a two-dimensional antisymmetric map *J. Phys. A: Math. Gen.* **27** 5187–200